European Journal of Remote Sensing

ISSN: (Print) (Online) Journal homepage: https://www.tandfonline.com/loi/tejr20

Multiple-input multiple-output radar, ground-based MIMO SAR for ground deformation monitoring

Francesco Mugnai & Dario Tarchi

To cite this article: Francesco Mugnai & Dario Tarchi (2022) Multiple-input multiple-output radar, ground-based MIMO SAR for ground deformation monitoring, European Journal of Remote Sensing, 55:1, 604-621, DOI: 10.1080/22797254.2022.2141660

To link to this article: https://doi.org/10.1080/22797254.2022.2141660

Published online: 17 Nov 2022.

EUROPEAN JOURNAL OF REMOTE SENSING
2022, VOL. 55, NO. 1, 604–621
https://doi.org/10.1080/22797254.2022.2141660

Multiple-input multiple-output radar, ground-based MIMO SAR for ground deformation monitoring

Francesco Mugnai[a] and Dario Tarchi[b]

[a]Department of Civil and Environmental Engineering, University of Florence, via di S.Marta, 3, 50139, Firenze, Italy; [b]Demography, Migration and Governance, Joint Research Centre, Via E. Fermi 2749, 21027, Ispra, Italy

ABSTRACT

This study focuses on investigating the capabilities of a Multiple-input multiple-output RADAR. A Radar interferometer, based on an electronically scanned array in MIMO configuration (MIMO-SAR), has been assessed for operational use in monitoring phenomena of geological interest, such as landslides unstable slopes. The system applies the very well-known and proven Ground-Based Interferometric technique. It guarantees a very short refreshing time compared to traditional systems based on the mechanical movement of the radar transceiver on a rail or the mechanical steering of a real antenna. The system can monitor several phenomena having deformation rates too high to be correctly retrieved by traditional systems currently in use. Implementing a prototype termed MELISSA allowed the testing technique's performances in two real case studies: a landslide and an unstable volcanic flank. The experimental results were compared with LISA, a well-known Ground-Based Interferometric Synthetic Aperture Radar (GBInSAR) interferometer. MELISSA allows for obtaining an excellent accuracy, better than 0.01 mm. The range and angular resolution are on the same order of magnitude as those obtained through LISA. However, the refreshing rate obtained from MELISSA, 0.01 s, guarantees a strong coherence even in challenging environmental scenarios as a flank of an active volcano.

ARTICLE HISTORY
Received 15 August 2022
Revised 30 September 2022
Accepted 24 October 2022

KEYWORDS
MIMO; SAR; GBInSAR; ground deformation; monitoring

Introduction

Synthetic Aperture Radar (SAR) interferometry is a well-known remote sensing technique that offers interesting applications (Bamler & Hartl, 1998). It may be implemented through space-borne, airborne, and ground-based sensors (Pieraccini et al., 1998), thus providing relevant information at different spatial scales from the global to the local one.

A typical application of the technique is the assessment of ground surface displacement fields over vast areas (Crosetto et al., 2005), whose first successful demonstration, using space-borne observation dates to more than 25 years (Besoya et al., 2021; Massonnet et al., 1994; Massonnet & Rabaute, 1993; Zebker et al., 1994). The technique is compelling in providing information on "changes detection". By comparing two observations (interferometric pair) of the same scene, made in different moments, the portions eventually experiencing modifications in the elapsed time between the observations can be identified and characterised. The nature and the amount of in-formation that can be retrieved strongly depend on the "coherence" of the observed scene (Izumi et al., 2021; Soni et al., 2021). The coherence has a precise mathematical formulation, and it is usually assumed that it measures the changes that occurred in the time interval (Maresca et al., 2021). We have to take into account the fact that the scene may also change during the acquisition of each observation forming the interferometric pair also due to atmospheric screen effect on propagation (Ichoku et al., 1998; Luzi et al., 2004; Tzouvaras, 2021).

Similarly, to the exposure time for an optical picture, the acquisition time for a SAR image plays a fundamental role in governing the quality of the image, what type of phenomenon can be observed and the quantity and quality of the retrieved information. This will impact the resulting coherence determining the information content about the occurred changes, which may pass from qualitative to quantitative. This may finally result in a precise determination of the contribution to the changes due to the displacement, namely the variation of the distance sensor-target along the Line-Of-Sight (LOS), with very high accuracy.

It is crucial to consider the sensor's frequency of observation and the corresponding wavelength when assessing the adverse effects on the image quality due to displacements of portions of the observed scene during its acquisition. Whenever the entity of the displacements occurring during the acquisition time becomes comparable with the wavelength, the

CONTACT Francesco Mugnai francesco.mugnai@unifi.it Department of Civil and Environmental Engineering, University of Florence, via di S.Marta, 3, 50139, Firenze, Italy

coherence of the portion is severely reduced and will not be correctly imaged. In summary (Prati et al., 1998), the resulting image quality mainly depends on the combination of three factors: i) the entity of the displacement with respect to the phase accuracy related to the wavelength; ii) the time interval necessary for the displacement to reach a value comparable to the accuracy of the measurement (correlation time); iii) the time to acquire the image (acquisition time).

Consequently, changes that develop quickly with a potentially severe effect on the coherence may be correctly imaged if the acquisition time is short enough. Shortening the acquisition time of a SAR image allows refinement of radar interferometry in traditional applications and makes new applications possible.

Considering the specific context in which the Ground-Based Radar Interferometry is used (Antonello et al., 2008; Leva et al., 2003; Massonnet et al., 1994; et al., 1994;Tarchi, 2003), it is now possible to consider a different approach, no longer based on the mechanical movement of the radar sensor, for implementing the SAR principle. A class of Ground-Based radar interferometers is implemented using the well-known concept of antenna array combined with an efficient switching system able to channel the signal to the different transmitting or receiving elements composing the array. An efficient way to implement this is offered by the Multiple Input Multiple Output (MIMO) technique (Bliss et al., 2006; Hosseiny et al., 2021; Hu et al., 2021; Jin et al., 2010). This approach and its equivalence to a traditional SAR approach have been demonstrated and experimentally validated (Massonnet et al., 1994). Even though alternative methods to realise an electronically scanned array exist, we will use the acronym MIMO-SAR after this to indicate this class of instruments. A fully working prototype has been implemented at the Joint Research Centre of the European Commission, and it has been extensively used to monitor the Costa Concordia wreck at the Giglio Island (Broussolle et al., 2014). In operational conditions, the system acquired images with an acquisition time of about 0.1 seconds, but the laboratory test, demonstrated to acquire up to 150 frames per second. The MIMO-SAR is not originally conceived and designed for GBInSAR application in a geological context, where a traditional approach has demonstrated its capability until maturity, making those systems a standard operational tool to measure ground displacements (Y. Deng et al., 2020; Feng et al., 2019; Han et al., 2019; Hu et al., 2021; Shi et al., 2021; Wasowski & Bovenga, 2022).

Consequently, the work reported here has the primary goal of assessing whether a similar system, bringing the capability of a very short acquisition time, may improve the monitoring of various phenomena of geological interest.

The work analyses the actual validated capabilities of MIMO-SAR concerning other existing approaches/systems currently used, analysing several real cases, including landslides and various types of slopes instabilities in a volcanic environment, where the monitoring with GBInSAR techniques is being performed. This analysis is then complemented by real tests, executed with the existing prototype that provided evidence of the advantages and limitations of MIMO-SAR. By combining the two types of analysis, it is finally possible to identify some scenarios where MIMO-SAR may represent a real advantage. In addition, it has also been possible to suggest further lines of research aiming at improving the MIMO-SAR by creating a version tailored for the use in a geological context, which helps, in synergy with another existing system, to extend further and enrich the monitoring capabilities of GBInSAR techniques. The MIMO-SAR has new and original capabilities, but its optimal use is combined with a traditional system since this is still the more efficient solution for many phenomena monitoring.

Materials and Methods

The Multiple Input Multiple Output (MIMO) approach

Research in Waveform-Diversity MIMO (WD-MIMO) radar systems (Friedlander, 2013; Li et al., 2007) has shown that it is possible to synthesise an arbitrary antenna array starting from opportunely spaced single elements by transmitting different waveforms at the element level and at the same time (Bliss et al., 2006; Curlander et al., 1991). In this case, the spacing between the elements is not requested to be relatively narrow, that is, comparable with the wavelength, but on the contrary, allows a higher degree of flexibility in designing the antenna array. A few industrial and economic operators have started to investigate the increased potential of this additional flexibility aiming to deliver innovative or alternative services to niche or new markets. This technique requires identifying each transmit element utilizing its specific waveform in its conventional implementation. This technique differs from the Space-Diversity MIMO (SD-MIMO; Wennstrom et al., 2001) radar system, which exploits angular diversity to acquire independent measurements of the Radar Cross Section (RCS) and increase in some ways and under different points of view the performance of the overall system (P F Sammartino et al., 2007). In the latter configuration, this MIMO radar system is the same as a radar network where the transmitters and the receivers, which can be co-located in pairs or not, are generally widely separated from one another. It has been shown (P F Sammartino et al., 2008) that this

MIMO system can outperform conventional monostatic radars under different points of view even if the overall Effective Radiated Power (ERP) is kept constant and with a reasonable increase in complexity. However, it is not convenient to consider this kind of MIMO for short-range SAR imaging purposes, and consequently, the developments exposed in this report are focused on the WD-MIMO, which is more suitable for a combination with the conventional antenna array concept.

WD-MIMO allows to dramatically reduce the number of antennas in transmitting and receiving, but to keep the overall performance of the system comparable to a conventional Electronically Steered Array (ESA; Moffet, 1968), whose application has been limited, so far, to relatively expensive sectors, due to the requested performances and high costs.

The idea of a minimum redundant array shown in (Farina, 1992) has been prodromal to these systems. Figure 1 shows a schematic of a minimum redundant array where some of the antennas of a conventional ESA can be removed, keeping the performance comparable with the original system

Figure 2 explains in more detail this concept: when the same waveform is transmitted, the non-Nyquist spacing in transmission generates grating lobes, which are compensated by the nulls of the pattern in receive, so that the resulting overall pattern is the same as a Uniform Linear Array (ULA; Yin & Zhang, 2020; Zhang et al., 2015) where one element only transmits and all of them receive. Consequently, if M antennas transmit and N antennas receive in a minimum redundant array configuration, the overall pattern is comparable to a linear array with MN receivers.

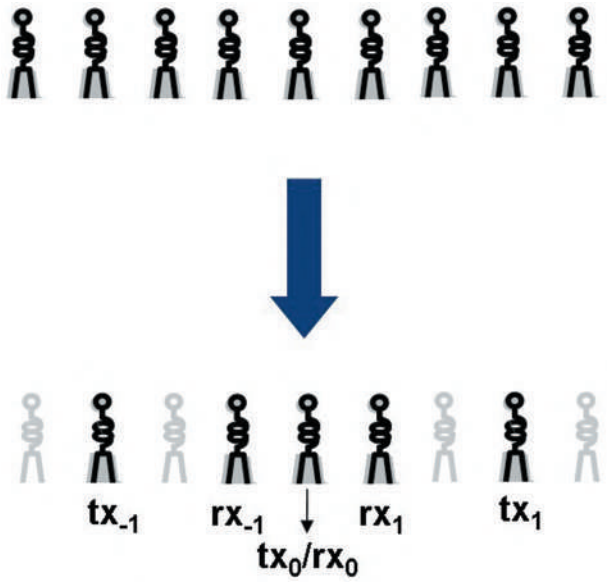

Figure 1. From a conventional antenna arrangement of an ESA to minimum redundant array and WD-MIMO antenna arrangement.

Notwithstanding this benefit, this comes with a cost. In conventional radar applications, minimum redundant arrays may not suit the routine tasks of a conventional ESA completely, as they suffer a reduction in the number of actual degrees of freedom in transmission and receive from MN (ESA) to M + N only (WD_MIMO). A WD-MIMO is less expensive and less complex than a ESA. Furthermore, it can deliver an increased flexibility if compared with a ESA, especially for some applications, such as detecting moving targets or working within a narrow area. One of the critical preconditions of the WD-MIMO technique is the possibility to

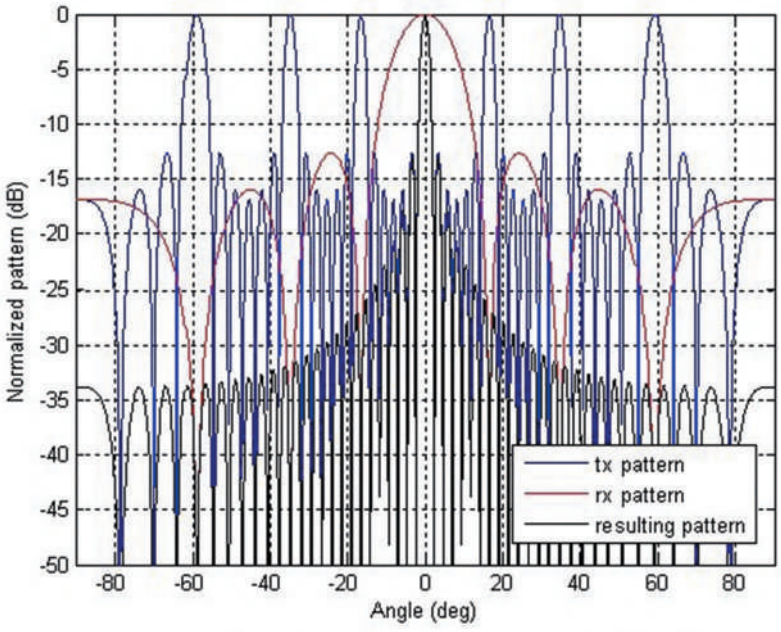

Figure 2. Example of simulated antenna pattern for a minimum redundant array beamforming (tx = TX, rx = RX).

distinguish the signals radiated from each antenna (e.g. through the employment of codes or separation on time). Under this assumption, it has been demonstrated (Bliss et al., 2006) that the array behaves similarly to a conventional ESA, yet (i) controlling a much smaller number of elements and (ii) gathering information from all the angles, which can be discriminated through receive-beamforming.

This is the core of the concept of WD-MIMO radars and explains the increasing interest in this technique as applied to various systems and is being considered a more-than-fair trade-off with the cost of avoiding beamforming in transmission.

Conventionally, a linear WD-MIMO system is being implemented as comprised of N receivers spaced at λ/2 and M transmitters spaced at Nλ/2 (or vice-versa; P F Sammartino et al., 2010; Pier Francesco Pier Francesco Sammartino et al., 2013). This configuration originates in receiving a linear shift of the phases from a single target, allowing focusing in data-processing and detecting targets at different angles without the need to scan the system or steer the beam.

It also seems important to clearly highlight that in WD-MIMO radars, orthogonality of the transmitted waveforms is a requirement for allowing signal separation at the receiver. However, it must be pointed out clearly that, as the waveforms are to be applied to radar systems, the requirement of orthogonality as intended in conventional communication systems, i.e.

$$\int_0^T w_m(t) w_k^*(t) dt = 0 \qquad (1)$$

where w_m (t) and w_k (t) are two different waveforms limited between 0 and T, and * is the conjugate operator, is a necessary condition even if it is not sufficient.

Other properties, such as mutual low-cross-correlation (H. Deng, 2004), good Doppler tolerance (Khan & Edwards, 2006) and good range resolution, are highly desirable to ensure the correct operation of these systems to outperform to some extent the conventional Electronically Steered Array (ESA). In summary, rather than moving the antennas on a rail, following the MIMO approach, it is necessary to install arrays of transmitting and receiving antennas at preselected distances, namely according to a precise antenna topology. Sequentially switching appropriately through the transmitting and receiving arrays then implements the antenna synthesis. An efficient antenna topology, composed by standard horn and Vivaldi antennas (Langley et al., 1993), is depicted in Figure 3.

To understand the above-mentioned increased flexibility and the potential of the design of MIMO systems versus conventional rail-mounted systems and ESAs, we assess the characteristics of this arrangement and compare it with a traditional synthetic array like for the actual LISA we introduce the concept of equivalent phase centre. For each possible couple of TX-RX antennas, the phase centre is the point having x = (TXx+RXx)/2 and y = (TXy+RXy)/2. We term it equivalent since the signal recorded by this TX/RX couple is approximately equivalent, at least in the far-field condition, to a couple of TX/RX modules co-located in the point. Due to the chosen spacing for TX and RX elements, phase centers are equally spaced at λ/4, which is the condition to fulfil Nyquist for any point arbitrarily chosen in the observed scenario. Central positions of the RX arrays are symmetrical and must be chosen to have the equivalent phase centres uniformly distributed with the proper spacing. It turns out that RX arrays overlap the TX elements at

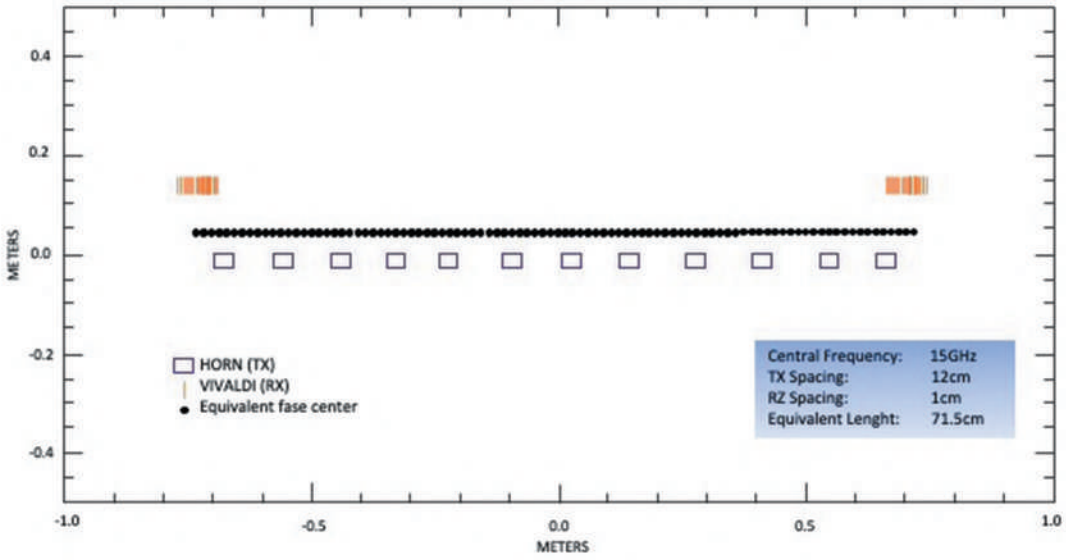

Figure 3. Front view of an antenna topology with TX (12 elements) spacing of Nλ /2 and RX (24 elements) spacing of λ/2. Two RX arrays are placed symmetrically in a lateral position.

the end of both sides, and consequently, they must be slightly separated along the Y direction, as in Figure 11.

It is important to note how the actual arrangement is highly effective in the ratio between equivalent aperture and physical dimension, which are now comparable in size. As a result, with only a fraction of the elements of a conventional antenna array, it is possible to design a system with an increased potential than the traditional rail-mounted system.

Expected advantages and limitations

A similar approach can, in principle, guarantee some benefits, for instance:

(1) It removes all the problems related to the mechanical rail's use (reliability, maintenance) and related controller.
(2) Secondly, eliminating the mechanical movements may dramatically improve the acquisition speed so that the number of images, which is now possible to gather, is significantly increased.

As mentioned above, this can be achieved generating several waveforms that are orthogonal to one another or, alternatively, it may consist of increasing the acquisition speed for the system relying on the use of a time-effective switching system. (Broussolle et al., 2014). This second solution makes it possible to emulate the generation of different codes utilizing a time and antenna division access to the channel. Although sub-optimal, if compared with the first solution, there can still be a great deal, as one waveform only is employed, reducing the costs associated with the generation and managing a variety of codes. Concerning the current state of play of the market and the state–of–the–art, cost-effective solutions are today available, making possible the implementation of a similar system provided that an efficient calibration procedure is identified and implemented as detailed in the following paragraph.

MELISSA – The prototype

The MELISSA system (Figure 4), implemented by the JRC, belongs to a new class of devices not based on the mechanical steering of the antenna system. MELISSA is a highly innovative and low-cost radar device system exploiting the MIMO concept to produce high-resolution coherent radar images. The novelty element of MELISSA is its unprecedented fast acquisition and refreshing times. The system can achieve a refreshing time smaller than 4 ms in its current implementation. MELISSA combines this new distinctive feature with all the other traditional advantages of a radar system,

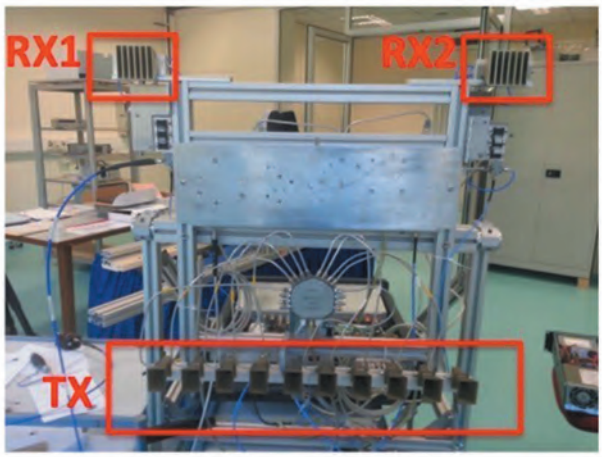

Figure 4. Picture of the MELISSA system (front side) with the indication of the two RX blocks and the transmitting array.

such as the day and night and all-weather capability. Moreover, the interferometric capabilities, typical of a coherent radar imaging system, are preserved, and faster phenomena can be precisely monitored.

Principle

As mentioned above, MELISSA can provide SAR images of the observed scene at a very high rate. Such an image has two dimensions: the range along the y-axis of the reference system depicted in Figure 5 and the cross-range or azimuth along the x-axis of the same system.

The range resolution is obtained through a Frequency-Modulated Continuous Wave (FMCW; Meta et al., 2007; Figure 6) de-ramping range compression process and is inversely proportional to the bandwidth.

On the other hand, advanced MIMO SAR processing achieves the resolution along the cross-range direction. The appropriate design of the array geometry allows gathering signals like those collected by a conventional array of N × M elements with N + M physical elements.

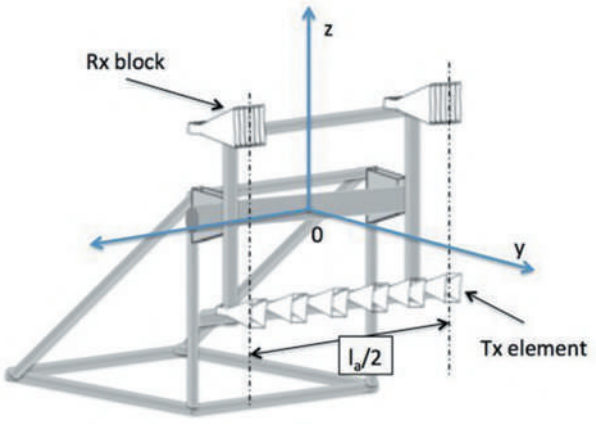

Figure 5. The geometry of the system MELISSA.

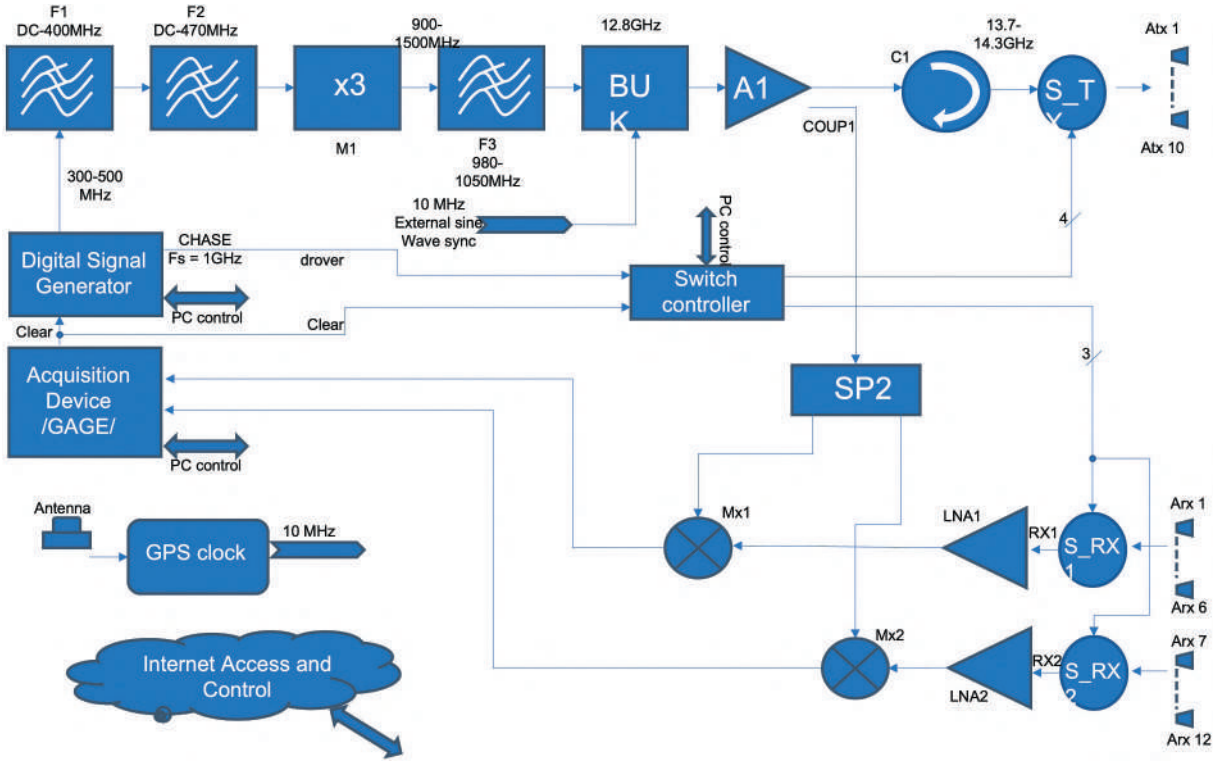

Figure 6. Scheme of the FMCW MIMO architecture.

The receiving part of MELISSA uses two blocks of N/2 antennas positioned at the two opposite sides of the transmitting array. The antennas are spaced by half the wavelength in the two receiving blocks. The transmitting part is formed of M (M = 10 in Figure 6) antennas spaced by a distance equal to the width of one receiving block. As a general principle, this is not the only configuration to place the antennas, yet it can be demonstrated (P F Sammartino et al., 2011) that it allows maximising the synthetic aperture and consequently improving the angular resolution of the system.

MELISSA performs radar measurements sequentially using all possible combinations of the M transmitting and the N receiving elements to achieve resolution along the azimuth direction. This is equivalent to forming a synthetic aperture *la* equals NMλ/2 (Massonnet et al., 1994), i.e. twice the distance between the centres of the two receiving blocks.

For each pixel in the image, MELISSA provides the amplitude and the phase measurements of the backscattered radar signal. The displacement ΔR of each pixel is estimated through the phase difference Δϕ of the backscattered signal in two consecutive images. The motion is measured against the Line Of Sight (LOS) direction using the relation $\Delta R \approx \lambda\Delta\phi/4\pi$, where λ is the wavelength and Δϕ is the phase difference. It is essential to notice that the LOS direction is the vector joining the phase centre of the radar antenna to the observed target. Consequently, each pixel of the image has a different LOS direction.

Theoretical accuracy

The theoretical limit of the accuracy $\delta(\Delta R)$ in measuring the displacement is obtained from the Cramer Rao Bound on the phase estimation as (Le, 2002; Van Trees, 1968):

$$\delta(\Delta R) \approx \frac{1}{4\pi\sqrt{2SNR}} \tag{2}$$

The expression of the signal-to-noise ratio after the image formation has to be considered (2) to the radar parameters. The SAR radar signal-to-noise ratio for spatial impulse target with given radar cross-section is given by (Curlander & McDonough, 1991):

$$SNR_1 = NM\frac{P_t T_{chirp} G_t G_r \lambda^2}{K_b T_0 F (4\pi)^3 R^4 L}\sigma \tag{3}$$

Where:

SNR_1 is the signal to noise ratio in the case of a point target

Pt is the transmitted power

T_{chirp} is the duration of the chirp signal

K_b is the Boltzmann constant

T_0 is the radar temperature.

F is the Noise factor of the receiving chain

R is the range of the target

L is the loss factor

G_t and G_r are the gain of the transmitting the receiving antenna, respectively

σ_0 is the normalised radar cross-section of the uniform observed zone

σ is the radar cross-section of the target
λ is the wavelength.

A point target is a small RADAR target compared with the pulse volume.

Results

This section reports some measurements performed by the MIMO- SAR prototype MELISSA in in-field conditions. They include two different phenomena, that is, a landslide and slope instability in a volcanic area, executed in different monitoring conditions. Each example has been selected and carefully analysed to validate some of the expected new peculiarities of a GBInSAR system experimentally with fast acquisition capabilities, as discussed in the previous sections based on theoretical considerations and tests in a controlled environment. Collectively, they provide the final element to perform a comprehensive assessment and definition of the optimal use of the new approach. To this aim, whenever possible, the measurements have been performed in combination with a traditional GBInSAR system (LISA). The performed measurements are briefly summarised in the following:

- Monitoring the Vetto landslide RE (Italy) – This was the first example of applying the MELISSA on a landslide. The campaign has been carried out in a site already continuously monitored by a LISA system; the area extends for four hectares. It was then possible to perform a first direct comparison of the capabilities of the two systems.
- Monitoring the slope instability on the Stromboli Volcano is the second example of application to a landslide but in a very different environment. As discussed in the previous section, various phenomena may benefit from using a system like MELISSA in a volcanic environment. This experiment, through a direct comparison with measurements performed by a LISA system, provides a first indication of the advantages that can be obtained in an adverse environment where several factors may strongly reduce the coherence of the observed scene, making it difficult also the acquisition of a single image. This campaign also allowed to refine the operation modes of the system further.

Monitoring of the Vetto landslide

Site description

The selected site (Figure 7) is located near Vetto (RE, Italy) is affected by an active landslide.

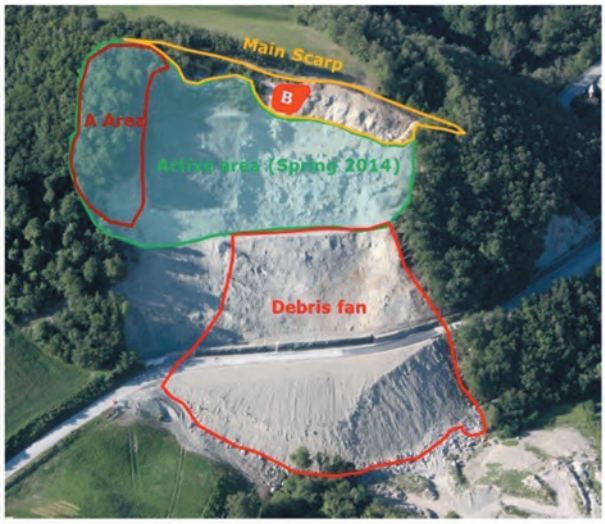

Figure 7. Aerial picture of the Vetto landslide.

The most active area is the prominent scarp of the landslide, and a sub-vertical E-W crack and parallel characterises it to the slope crest. The presence of historical and recent gravitational movements is witnessed by striaes, slicken-sided and riedel type calcitic accretions on the surfaces.

On the slope base a main regional fault connects Epiligurian formations (Pantano, Antognola/Contignaco) with the Ligurian one (Argille Varicolori; Bertolini & Pellegrini, 2001). This can be interpreted as a clue of the tectonic origin of the discontinuity, considering the parallelism with the main regional fault. The recent landslide activity is nevertheless attributable to the gravitational pull.

The slope is composed in the upper part by marls (Antognola) and by sandstones in the lower one. Strata run counter to the slope with a high deep (from 60° to 70° south). The rock mass in the north part of the main crack is highly fragmented, probably due to the historical gravitational deformation.

The main scarp shows a differential displacement amongst the upper part, and the lower one, the first, is affected by an intense displacement.

The rupture surface is visible in the ridge and disappears in the slope, showing minor deformation but more pervasive. Furthermore, the rupture surface is evident in the central part of the slope where the lithologic transition between Marles and Sandstone and where major blocks detachment happened.

Two secondary local effects also must be mentioned:

Scratches and disordered displacements act with a metric value in the A zone steps. Such a context could lead to a higher instability degree. In the B zone, the peculiar joint distribution defines a rock portion of about 1000 cubic meters. This rock volume is unconfined and shows a high cinematic freedom degree.

The campaign aimed to perform a test of the MELISSA's capabilities for the monitoring of

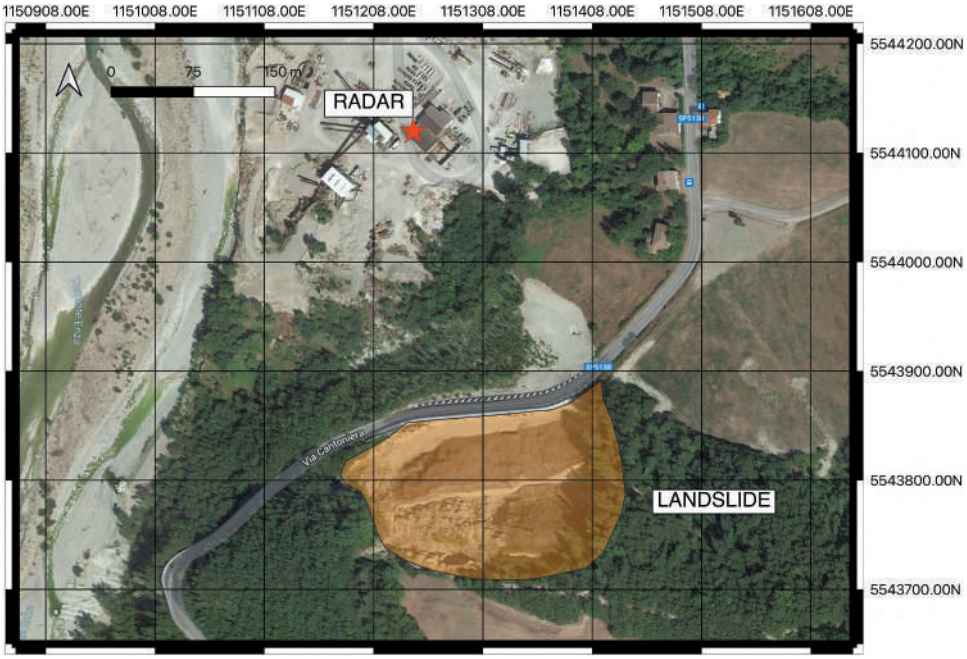

Figure 8. Satellite view showing the position of the devices (RADAR) and the landslide (Orange area).

a landslide in operative conditions. The site was already under continuous monitoring with a traditional GBInSAR system (LISA) so that data collected with an existing and validated technology to be used for a direct comparison were available.

The MELISSA system has been installed to be as close as possible to LISA and has a similar LOS concerning the slope under study to make the data comparison more reliable. The distance for both systems to the affected area was from 130 to 370 m. The position of the MELISSA and LISA is shown in Figure 8

Figure 9 shows a picture of the landslide taken from the location of MELISSA.

Performed Experiments

Whilst the goal of the experiment was to obtain a series of interferograms from the MELISSA system to be directly compared to the ones obtained by LISA on the same time span, the sequence of planned experiments was also aimed at assessing the different performances of the system based on different acquisition parameters. It was of interest to:

- Compare results obtained by MELISSA with results from LISA in terms of capabilities to retrieve LOS displacements and correctly position them within the observed scene;
- Assess the dependence of these capabilities on the acquisition parameters such as the unambiguous range (i.e. maximum covered distance) and acquisition time. The data collection has been executed in eight different configurations as reported in Table 1 and according to the acquisition parameters in Table 2.

Figure 9. The landslide from the MELISSA system.

Table 1. Characteristics of the different acquired datasets.

Duration of the measurements	Maximum unambiguous range	Interleave between two images
10 min	1000 m	0.05 sec
1 h 6 m	1000 m	0.05 sec
5 min	400 m	0 sec
2 min	200 m	0 sec
5 min	2000 m	0 sec
5 min	4000 m	0 sec
5 min	1000 m	1 sec
5 min	400 m	0 sec

Table 2. Systems parameters for the measurements in Vetto.

Parameters	Symbol	LISA	MELISSA
Wavelength	λ	1.74 cm	2 cm
Radiated power (CW)	Pt	22dBm	22dBm
Total transmitted Bandwidth	B	200 MHz	345 MHz
Number of equivalent channels elements	M*N	601	120
Switch time	Tswitch	_	1.92 μs
Noise factor of receiving chain	F	_	5 dB
Range resolution	δR	0.80 m	0.43 m
Synthetic aperture length	la	3.0 m	0.80 m
Angle resolution	δθ	0.4°	1.3°
Swath	S	1.0 Km	0. 2-- 4.0 Km
Single chirp time	Tchirp	40 msec	20 -- 400 μs
Acquisition time	Ta	70 s	2.6 -- 50 ms

MELISSA recorded approximately 150.000 images in off-line mode, stored for post-processing.

Results comparison

The power SAR images obtained by the two systems are shown in Figure 10.

The result is quite similar, considering the significant difference in the length of the synthetic aperture that explains the lower azimuth resolution of the MELISSA system. All main relevant features in the observed scene are imaged similarly by the two systems, as is the case for the metallic fence (visible in Figure 10) and corresponding to the bright horizontal line at a range of about 240 m). The area from which a significant power is received is similar in both images, and a slight difference can be appreciated due to the slightly different installation position.

Figure 11a and 11b shows the displacement maps obtained over the same time interval of 65 minutes by LISA and MELISSA, respectively. The main area of displacement, highlighted by the white circles, is correctly identified similarly in both maps. The displacement pattern is the same spatial distribution and value along the LOS. Therefore, the white area within the white circle corresponding to phase wrapping in the

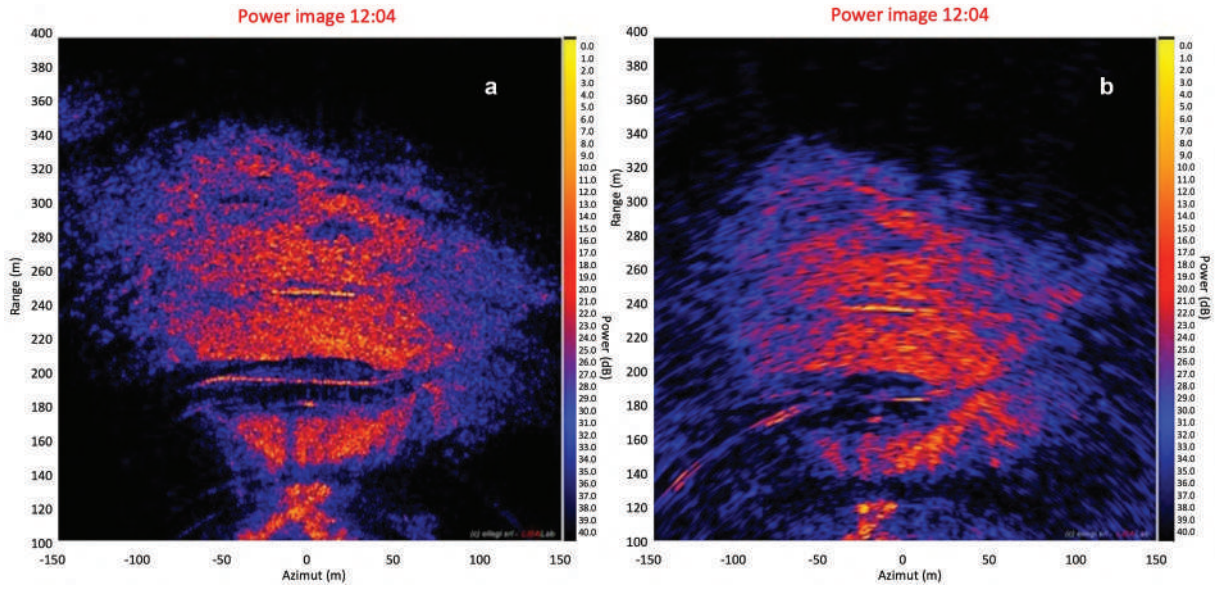

Figure 10. Power SAR image of the Vetto landslide: (a) produced with LISA; (b) produced with MELISSA. They appear comparable even though the spatial resolution is different (Table 2). It is noted that the acquisition time for LISA and MELISSA is 70s and .05s, respectively.

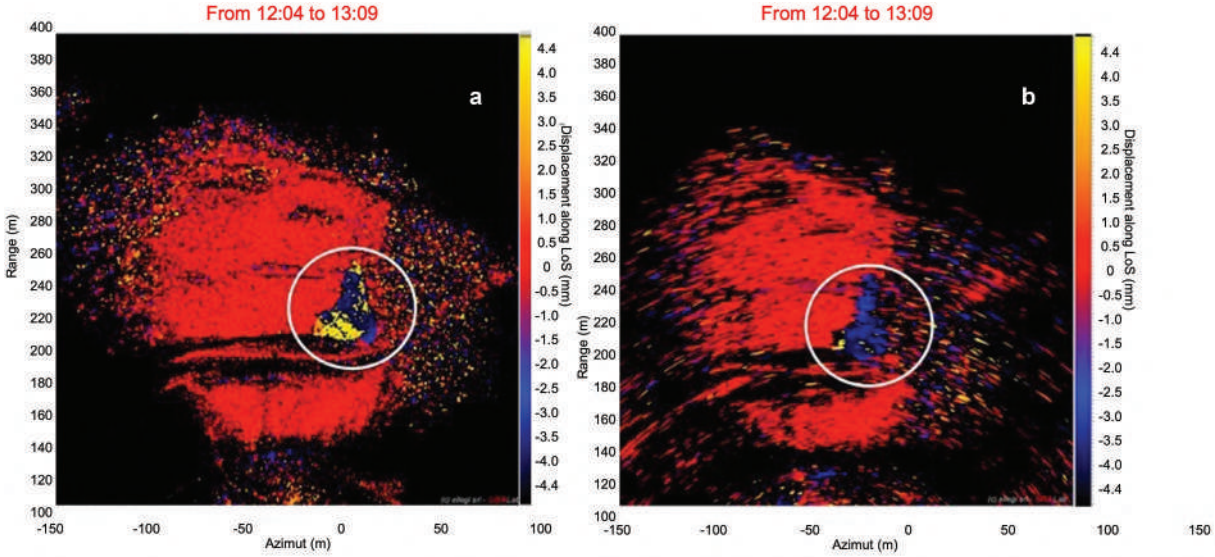

Figure 11. Displacement maps of the Vetto landslide: (a) produced with LISA; (b) produced with MELISSA. Both maps refer to the same 65 minutes time span. The white circle highlights the area where significant displacements are detected.

LISA map is larger than the map retrieved by MELISSA.

Figure 12a and 12b finally shows the displacement maps obtained over the same time interval of 65 minutes by LISA and MELISSA, respectively, but the LISA measurement has been now degraded to have a similar azimuth resolution as the MELISSA one. This comparison does not provide any additional information but allows appreciating how the overall loss of quality of the MELISSA image is due more to the lower azimuth resolution than the much shorter integration time. Concerning range resolution, the wider MELISSA wideband allows for a better performance than LISA.

Many additional tests have been performed to assess a possible dependency of MELISSA capabilities on varying measurement parameters, using the different datasets listed in Table 1. No significant variations have been recognised so that the results reported in Figure 12 can be considered representative of all different sets of acquired measurements.

Monitoring of the slope instability on the Stromboli Volcano

A second experimental campaign has been executed on the Stromboli volcano. The series of measurements reported here explicitly aimed at assessing the system's robustness against factors inducing short-term decorrelation effects, i.e. during a time frame comparable to the acquisition time of a single image and then

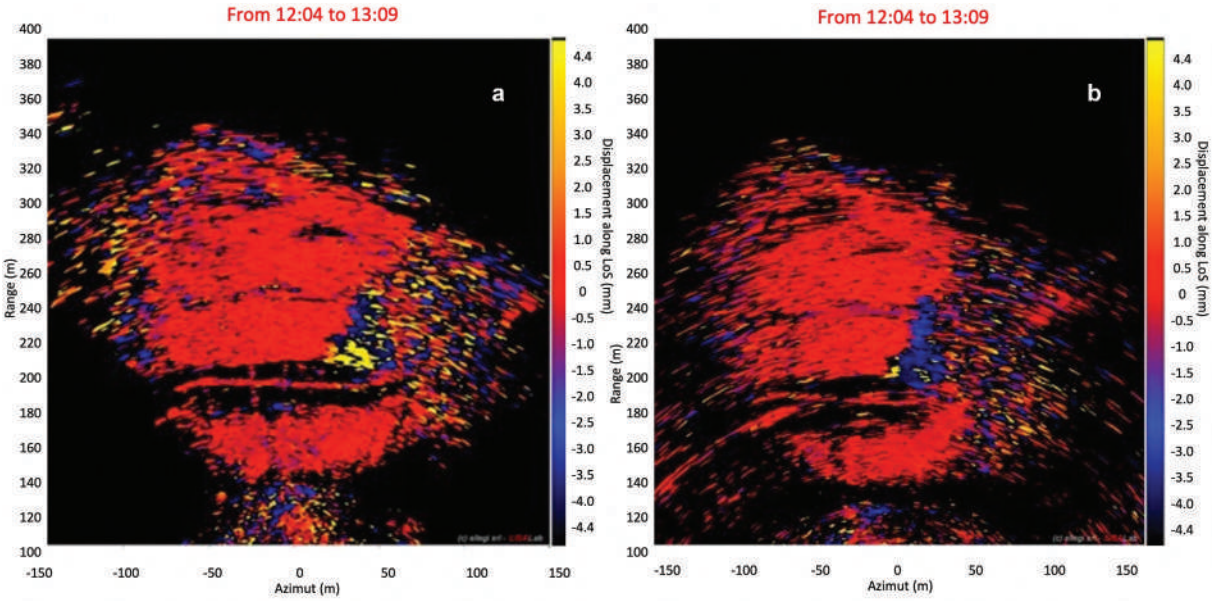

Figure 12. Displacement maps of the Vetto landslide: (a) produced with LISA; (b) produced with MELISSA. The LISA map now has a degraded resolution comparable with the MELISSA one.

strongly affecting its quality. The longer the typical acquisition time for an image the more prone could be the system to this problem.

Situations of this kind may often arise in Stromboli (Bevilacqua et al., 2020; Marsella et al., 2009), as the case in crater areas, as already reported in 3.1.3 and on the Sciara del Fuoco (SdF). In this area, an additional factor is related to superficial effects due to the continuous remobilization of the material. This factor directly induces short-term decorrelation of the observed area and, particularly in dry seasons, creates dust that may represent an additional source of phase shift.

The final effect may already be visible in the power strength of the radar signal. It can be appreciated by comparing the image displayed in Figure 13(a), acquired over the SdF during a period in which the phenomenon of concern has been observed, with the image in Figure 13(b), corresponding to a different time showing an excellent long-term coherence in the acquisition. The area indicated by the white circle appears somewhat degraded with an essential loss of reflectivity.

Even though the effect is not well evident in the power image, its SNR may be degraded, and this will become evident by calculating the coherence with a second image even very close in time, as shown in figure 60. The area corresponding to the SdF in Figure 14(a) exhibits an evident loss of coherence compared to a "normal" situation like in Figure 14 (b). In this specific case, the time span of the pair is the minimum possible for the system.

Under this condition, the system becomes virtually "blind", and it is impossible to provide any information about the deformation pattern of the area. The implications for the monitoring activities are crucial.

Consequently, by using much shorter acquisition times, the primary goal of the test was to assess whether a system like MELISSA may be able to overcome the problem affecting LISA and retrieve, even though over a limited time and limited areas, the actual deformation pattern.

MELISSA has been installed very close to the LISA system in the position displayed in Figure 15. The measurement parameters for the two systems are summarised in Table 3.

The measurements reported here covered a total timespan of about 8 hours. The first part of the test aimed to identify the longest acquisition time that can produce an image with acceptable SNR and the longest time span between the image pair, maintaining sufficient coherence. An acquisition time of 0.1 seconds has been identified as a value allowing obtaining a good quality image (Figure 16).

Figure 17 summarises the different tests executed to identify the optimal time interval between images. The coherence of a pair corresponding to 1 second time span (acquisition time of 0.1 s for each image) has an excellent coherence (0.95; Figure 17a), but the coherence reduces significantly (0.6) already over 2 min (Figure 17b). The optimal time span for the pair has been finally identified in 10 seconds.

With these parameters, a sequence of more than 2000 images has been acquired for a total duration of about 6 hours. The applied processing includes the following steps:

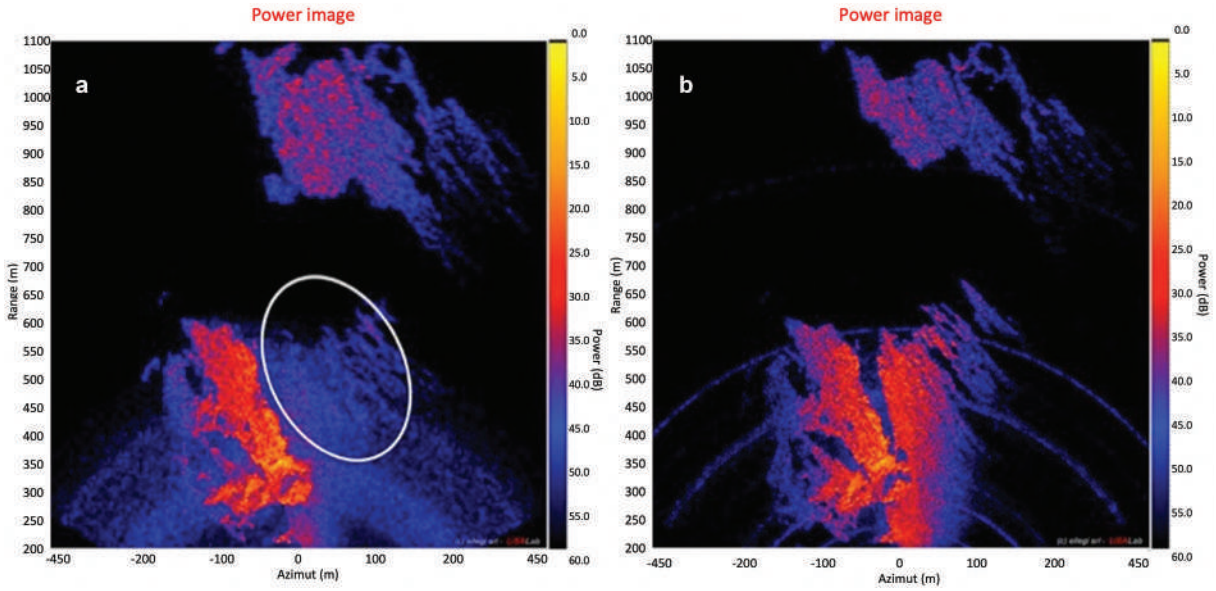

Figure 13. Power SAR images of Stromboli were acquired at a different time. (a) The image appears degraded in the area indicated by the white oval. (b) Reference image acquired in a period that is not affected by short-term decorrelation effects. (Courtesy by Ellegi Srl).

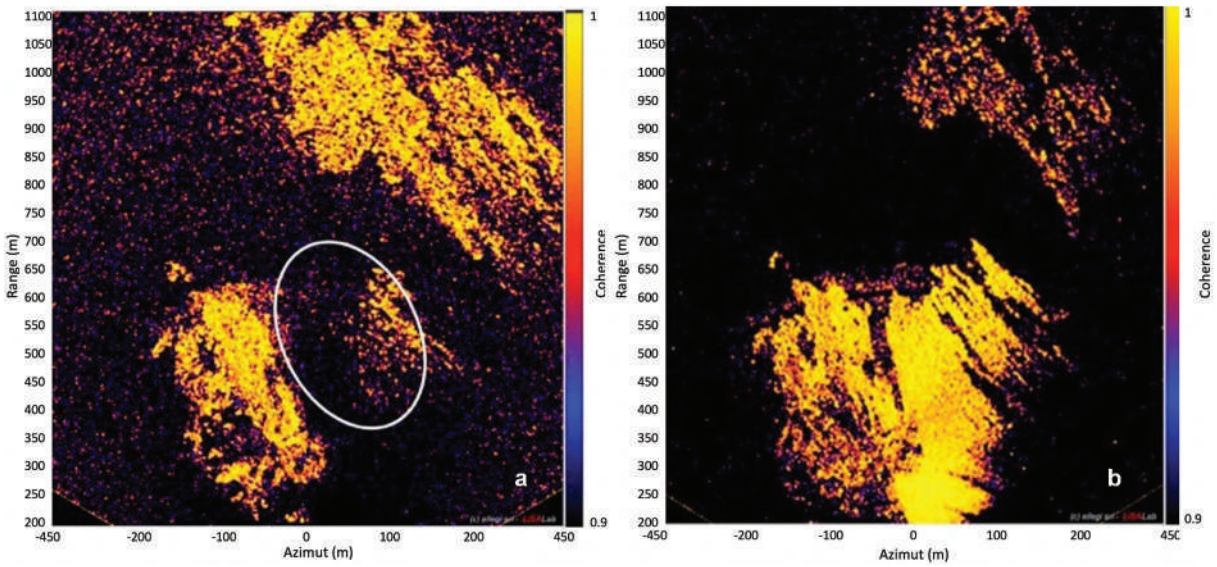

Figure 14. Coherence maps on Stromboli acquired in different periods. (a) the map is calculated over a time span of 22 min and corresponds to the same period as Figure 14a. The loss of coherence in different areas of the SdF indicated by the white oval is evident. (b) Reference coherence map acquired in the same period as Figure 14b. (Courtesy by Ellegi Srl).

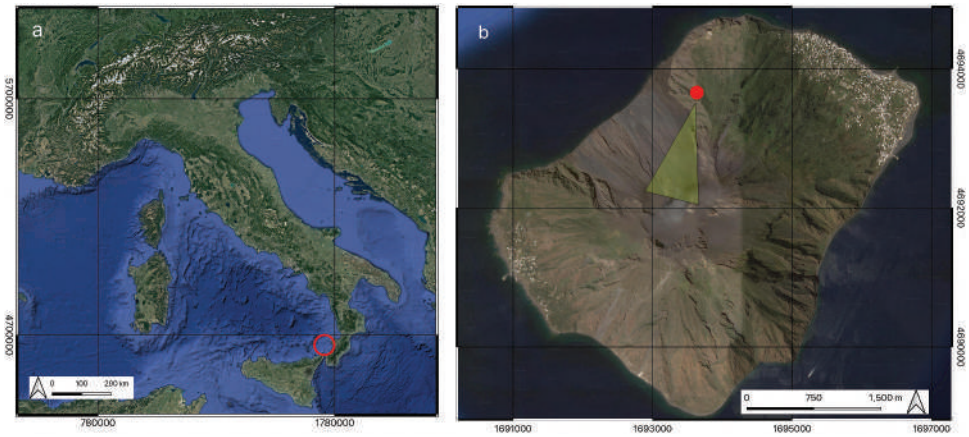

Figure 15. (a) Stromboli Island is in the southern part of Italy. (b) Set-up for the measurements campaign in Stromboli. The red circle indicates the position of the installation. (Courtesy by Ellegi Srl).

- The formation of interferograms using each possible pair of contiguous images ITFn.
- The derivation of the relative displacements map from each pair Dispn.
- The formation of a cumulative map by recursively adding up each new $Disp_n$: $Disp_{cum} = \Sigma$ Disp

The final cumulative map is shown in Figure 18.

It allows retrieving quite clearly an area affected by a displacement in the order of 2 mm (towards the observer). Such a value is coherent with the deformation pattern of the considered period, which is typical of a low volcanic activity (Di Traglia et al., 2014). The map appears to be quite noisy and requires additional spatial filtering (5x5 pixel), which decreases the spatial resolution but improve the final quality.

This has to be compared with the corresponding result with LISA, as shown in Figure 19.

The area corresponding to the SdF and the area in Figure 19 (squared white box) is affected by very high noise that prevents quantitative information retrieving.

Discussion

The campaign on Vetto Landslide represented the first case where the MELISSA system has been used to monitor landslides. A traditional LISA system, performing continuous monitoring of the same area, has provided validation data. The comparison of results showed a significant match. Interferograms elaborated through the acquisitions made on Vetto Landslide using LISA and MIMO SAR, were analysed. A substantial equivalence between the two instruments can be noticed from the accuracy point of view. In particular, the displacements detected in the

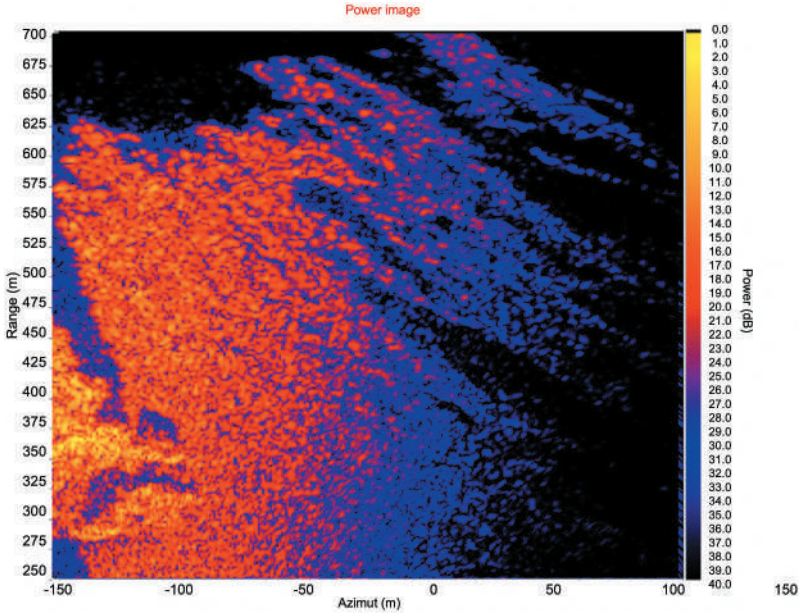

Figure 16. Power image of the SdF acquired with MELISSA with an acquisition time of .1 seconds.

Table 3. Acquisition parameters for the measurements in Stromboli.

Parameters	Symbol	LISA	MELISSA
Wavelength	λ	1.74 cm	2 cm
Radiated power (CW)	Pt	27dBm	22dBm
Total transmitted Bandwidth	B	100 MHz	200 MHz
Number of equivalent channels elements	M*N	601	120
Switch time	Tswitch	_	1.92 μs
Range resolution	δR	0.80 m	0.43 m
Synthetic aperture length	la	3.0 m	0.80 m
Angle resolution	δθ	0.4°	1.3°
Swath	S	2.0 Km	1.0 Km
Single chirp time	Tchirp	200 msec	800 μs
Acquisition time	Ta	640 s	0.1 s

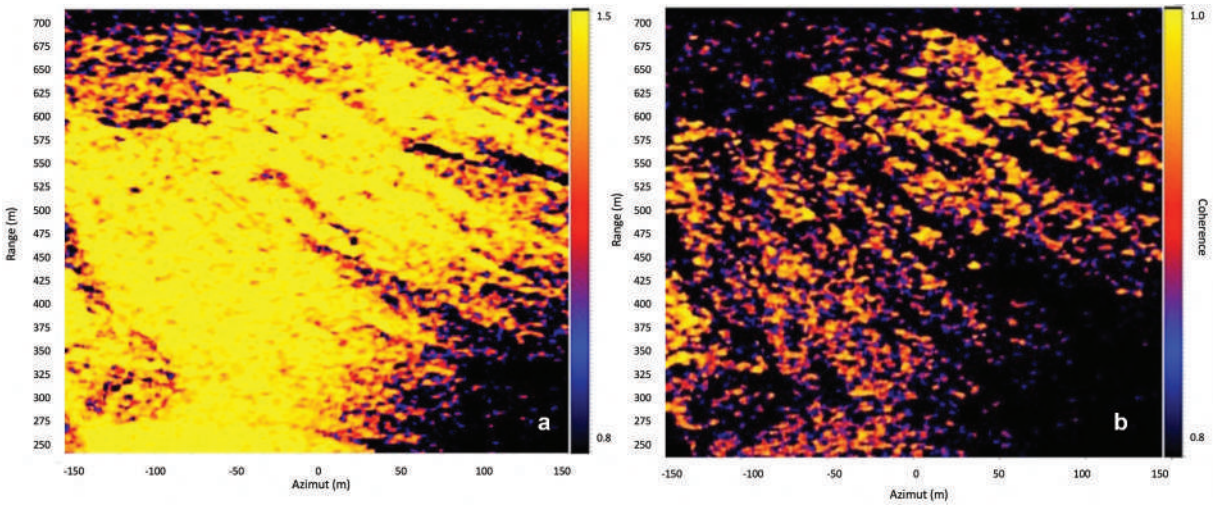

Figure 17. Coherence maps over a time span of 1 s and 2 min in (a) and (b), respectively. The loss of coherence in (b) is severe.

time span of 65 minutes vary between 2.0 mm and 4.4 mm for MIMO and GBInSAR. The maximum measurement accuracy of the MELISSA system has been experimentally assessed in laboratory about 0.01 mm (Broussolle et al., 2014). Considering the short time interval between the two radar images used for the interferogram formation, the atmospheric correction is not necessary and the measurement accuracy can be reasonably identified with the standard deviation estimated on stable points.

A brief resume of the results obtained during a monitoring period carried out with GBInSAR LISA

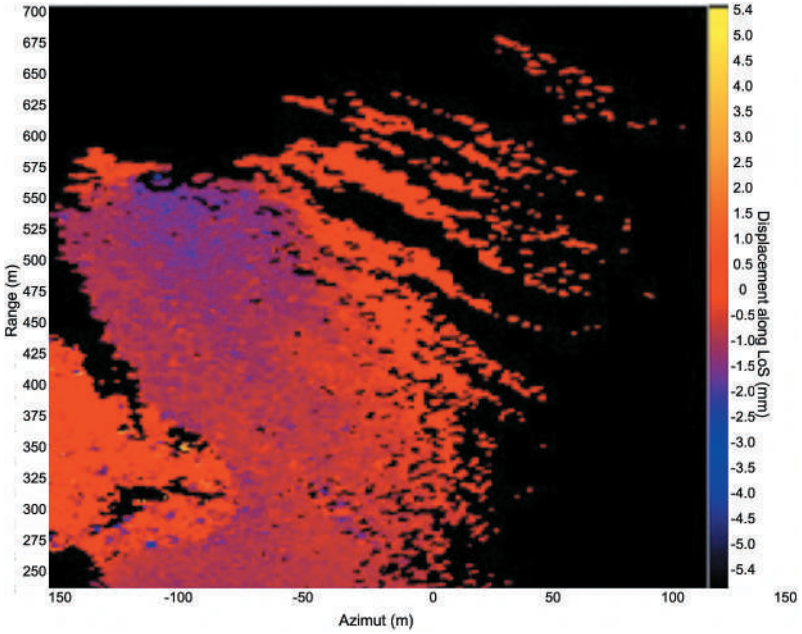

Figure 18. A cumulative displacement map over a time span of about 6 h was obtained by elaborating the entire dataset of images acquired (more than 2000). A spatial averaging filter (5 x 5 pixel) has been applied. A slight displacement (2 mm towards the observer) has been detected in the area corresponding to the SdF.

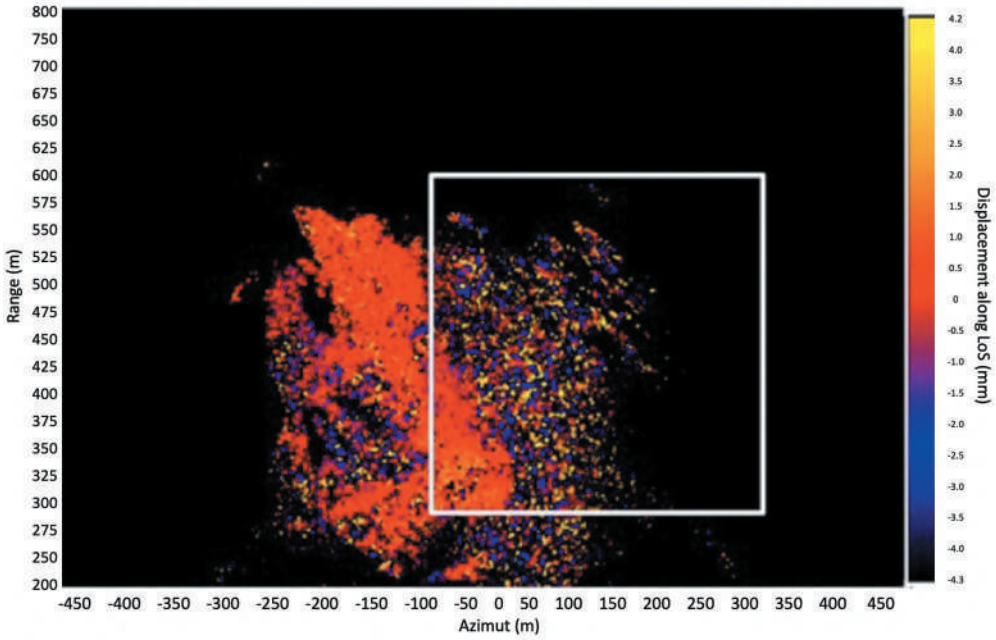

Figure 19. Displacement map obtained with LISA over the same time span as in figure 64. The white square indicates the area covered by MELISSA. The area corresponding to the SdF appears very noisy, and no information can be retrieved. (Courtesy by Ellegi Srl).

gives a short description of the landslide activity. The test of MELISSA was carried out during 8 hours within the period.

The Vetto Landslide has been monitored by LISA for 1 year. Considering the geological setting and the infield evidence, five warning points, were identified as representative of the landslide deformations (Figure 20).

Within 172 days, the landslide shows a deformative activity as shown in Table 4. The maximum deformation of 6116 mm was recorded on point 4.

The test carried out on Stromboli Island showed similar results from MIMO-SAR and LISA. The SdF had a "high" deformation activity in the monitored period, namely from 1.2 mm/day to 1 mm/hour as defined by (DI TRAGLIA FEDERICO et al., 2014). The results

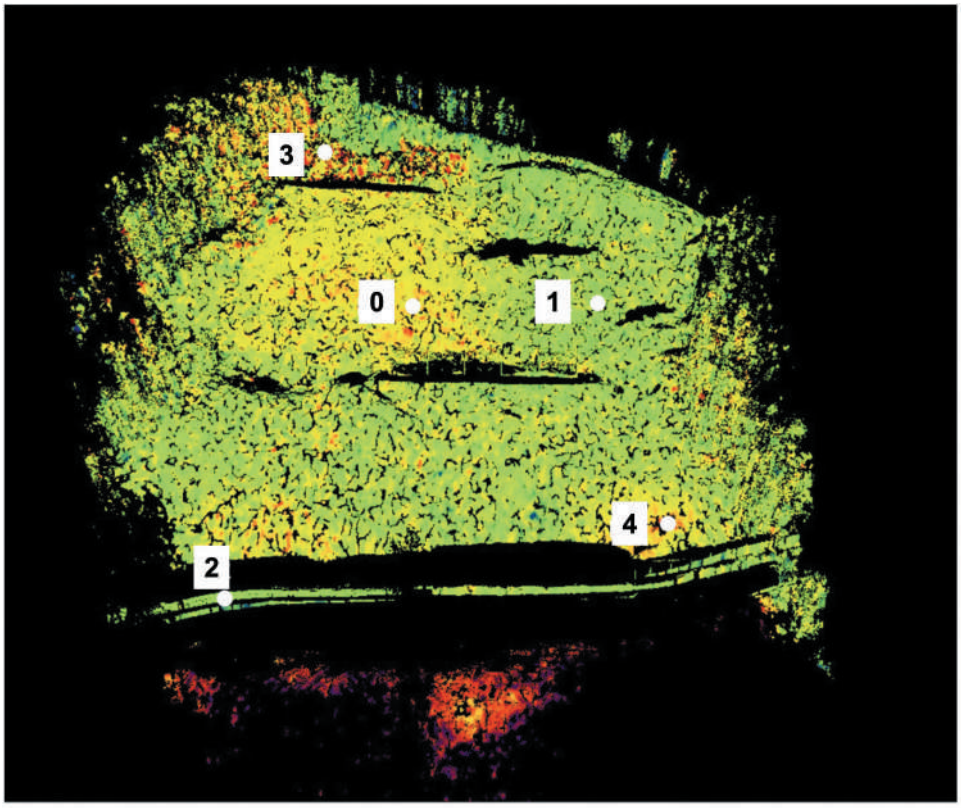

Figure 20. Frontal view of the 3D deformation model with the 5 warning points.

Table 4. Measured displacements on control points.

	Displacement (mm) 24 h	Displacement (mm) 172 days
Point 0	1.70	52.10
Point 1	0.20	1.90
Point 2	<0.1	<0.1
Point 3	0.70	228.40
Point 4	0.40	6116.30

from the monitoring test carried out with MELISSA within a time span of 6 hours shows a total deformation of 2 mm.

In this case, however, the quality of RADAR images obtained with MELISSA was higher than those obtained with the LISA System. The high refreshing time, which is 0.01 s, allows for good coherence even in the case of dusty and unfavorable environments as a flank of an active volcano.

Minor mismatches can be explained in slightly different aspect angles and spatial resolutions. MELISSA has a much lower resolution in azimuth due to the limited equivalent synthetic aperture that can be realized, resulting in lower overall image quality. Nevertheless, the system can correctly retrieve the displacement pattern compared to LISA, both spatial distribution and absolute values. Despite the much lower integration time due to the much shorter acquisition time, MELISSA achieved a sufficient SNR on the acquired images, that is, over a maximum range up to 400 m.

It must be underlined that the two power images shown in Figure 11 correspond to acquisition times of 70 s and 0.05 s for LISA and MELISSA, respectively.

The reported test validated MELISSA's capability to incorrectly retrieve the displacement pattern of an unstable slope with a very high refreshing rate but reveals the presence of new original issues that need to be fully addressed.

The most important is undoubtedly the considerable amount of data produced by the system due to the short acquisition time. In the reported campaign, 5 hours of monitoring produced an amount of about 120 Gb of data, corresponding to almost 180,000 images.

These data need to be stored and processed efficiently, considering the specific features of the phenomenon under monitoring. This additional test highlighted the need for a more comprehensive approach, which should effectively account for the total duration of the monitoring, a significantly short acquisition time and the quick availability (real-time) of results.

The campaign on Stromboli volcano has been crucial in providing several indications confirming the expected advantages of using a system like MELISSA in an adverse environment like the volcanic one.

It has been confirmed the possibility to overcome the severe limitations that a traditional system like

LISA may encounter in terms of loss of short-term coherence. The acquisition time that MELISSA can use turned out to be fast enough to approach the specific situation existing in Stromboli and modulate the measurement parameters to reconstruct the displacement pattern despite the presence of short-term solid decorrelation not allowing LISA to get comparable results.

On the other hand, it must be stressed that this appears to be a viable solution only over limited areas due to the limitations that distance imposes on the acquisition time and over a limited time span. The collected data is vast, and the related processing is highly demanding. There is a clear need to carefully analyse these aspects and develop a specific effective procedure. These measurements confirm excellent performances until 500-600 m in terms of attainable SNR in terms of operational range.

The overall conclusion is that MELISSA, based on its actual performances, brings clear advantages to the monitoring activities with GB-InSAR. It appears the ideal tool to complement a traditional system, but it can still not cover the full range of tasks that a monitoring system must ensure efficiently and advantageously.

Conclusions

An interferometer, based on an electronically scanned array in MIMO configuration (MIMO-SAR), has been assessed for operational use in monitoring phenomena of geological interest, such as landslides and unstable slopes. The system is, in principle, able to apply the very well-known and proven Ground-Based Interferometric technique. It may guarantee a short refreshing time, in the order of 0.01 s, in comparison with traditional systems, based on the mechanical movement of the radar transceiver on a rail or the mechanical steering of a real antenna. The prototype termed MELISSA has been applied in infield experimental campaigns. They include:

- A monitoring campaign of the Vetto landslide. This provided the first successful example of the application of the prototype on a landslide. The campaign has been executed in a site continuously monitored by a traditional system (LISA) and then compared the obtained results. The results turned out to match very well. Consequently, this test confirmed the expected good performances of the system in a range up to 500 m.
- A monitoring campaign of an unstable slope on the Stromboli Volcano. This is the second example of application to a landslide but in a very different environment. Again, it was possible to compare data with a traditional GBInSAR system. This test provided results in line with the previous case in general terms. More importantly, it has also shown the robustness of the MIMO-SAR concerning factors inducing a fast decorrelation of the observed scene and usually preventing the acquisition of good quality images.

A reference design for the MIMO-SAR able to ensure about 125 images per second in a maximum range of about 500 m turns out to be fully validated, and this also corresponds to the reference scenario for its operational use. In this scenario, the MIMO-SAR may acquire images with a high rate while it is equivalent to the existing system concerning other relevant measurement parameters. The MIMO-SAR performances start to degrade, increasing the distance, and it is impossible to maintain the same high rate of acquisition with equally good performances in terms of image SNR. For this reason, the first recommended scenario is in support and combination with a traditional system, providing a temporary close-in view over portions that exhibit an acceleration of the deformation rates. A second scenario concerning the provision of early warning is also provided, and this is particularly tailored for situations where a fast-evolving phenomenon may suddenly develop without clear precursors. Finally, possible options to enhance the system have been presented.

In conclusion, the MIMO-SAR approach may undoubtedly bring some original and, in some respect, unique advantages, which can further extend the field of applicability of the GB-InSAR technique for the monitoring of ground deformation. For the time being, its optimal use is in combination with and support traditional systems.

Acknowledgments

The authors want to thank: Ellegi Srl for technical support and GBInSAR instrumentation.

Data Availability

Data available on request from the authors. The data that support the findings of this study are available from the corresponding author, [Mugnai F.], upon reasonable request.

Disclosure statement

No potential conflict of interest was reported by the author(s).

Funding

This research received no external funding

ORCID

Francesco Mugnai http://orcid.org/0000-0002-4146-6443

Author Contributions

Conceptualization, Francesco Mugnai; methodology, Francesco Mugnai; software, Francesco Mugnai; validation, Francesco Mugnai; formal analysis, Francesco Mugnai; investigation, Francesco Mugnai; resources, Dario Tarchi; data curation, Francesco Mugnai; writing—original draft preparation, Francesco Mugnai; writing—review and editing, Francesco Mugnai; visualisation, Francesco Mugnai; supervision, Francesco Mugnai and Dario Tarchi; project administration, Francesco Mugnai and Dario Tarchi; funding acquisition, Dario Tarchi. All authors have read and agreed to the published version of the manuscript.

References

Antonello, G., Fortuny, J., Tarchi, D., Casagli, N., Del Ventisette, C., Guerri, L., Luzi, G., Mugnai, F., & Leva, D. (2008). Microwave interferometric sensors as a tool for space and time analysis of active volcano deformations: The Stromboli case. *Use of Remote Sensing Techniques for Monitoring Volcanoes and Seismogenic Areas, 2008*. USEReST 2008. *Second Workshop On*, 1–6.

Bamler, R., & Hartl, P. (1998). Synthetic aperture radar interferometry. *Inverse Problems*, *14*(4), R1. https://doi.org/10.1088/0266-5611/14/4/001

Bertolini, G., & Pellegrini, M. (2001). The landslides of the Emilia Apennines (Northern Italy) with reference to those which resumed activity in the 1994–1999 period and required civil protection interventions. *Quaderni Di Geologia Applicata*, *8*(1), 27–74.

Besoya, M., Govil, H., & Bhaumik, P. (2021). A review on surface deformation evaluation using multitemporal SAR interferometry techniques. *Spatial Information Research*, *29*(3), 267–280. https://doi.org/10.1007/s41324-020-00344-8

Bevilacqua, A., Bertagnini, A., Pompilio, M., Landi, P., Del Carlo, P., Di Roberto, A., Aspinall, W., & Neri, A. (2020). Major explosions and paroxysms at Stromboli (Italy): A new historical catalog and temporal models of occurrence with uncertainty quantification. *Scientific Reports*, *10*(1), 1–18. https://doi.org/10.1038/s41598-020-74301-8

Bliss, D., Forsythe, K., & Fawcett, G. (2006). MIMO Radar: Resolution, performance, and waveforms. *Proceedings of ASAP*.

Broussolle, J., Kyovtorov, V., Basso, M., Castiglione, G. F. D. S. E., Morgado, J. F., Giuliani, R., Oliveri, F., Sammartino, P. F., & Tarchi, D. (2014). MELISSA, a new class of ground based InSAR system. An example of application in support to the Costa Concordia emergency. *ISPRS Journal of Photogrammetry and Remote Sensing*, *91*, 50–58. https://doi.org/10.1016/j.isprsjprs.2014.02.003

Crosetto, M., Crippa, B., Biescas, E., Monserrat, O., Agudo, M., & Fernández, P. (2005). Land deformation measurement using SAR interferometry: State-of-the-art. *Photogrammetrie Fernerkundung Geoinformation*, *2005*(6), 497 .

Curlander, J. C., & McDonough, R. N. (1991). *Synthetic aperture radar* (Vol. 11). Wiley.

Curlander, J. C., McDonough, R. N., Sparr, T., Krane, B., Li, J., Stoica, P., & Cruden, D. M. (1991). Landslide Types and Processes, Special Report, Transportation Research Board, National Academy of Sciences. *SAR Image Analysis, Modeling, and Techniques V*, *4883*, 20–26.

Deng, H. (2004). Polyphase code design for orthogonal netted radar systems. *IEEE Transactions on Signal Processing*, *52*(11), 3126–3135. https://doi.org/10.1109/TSP.2004.836530

Deng, Y., Hu, C., Tian, W., & Zhao, Z. (2020). 3-D deformation measurement based on three GB-MIMO radar systems: Experimental verification and accuracy analysis. *IEEE Geoscience and Remote Sensing Letters*, *18*(12), 2092–2096. https://doi.org/10.1109/LGRS.2020.3014342

Di Traglia, F., Nolesini, T., Intrieri, E., Mugnai, F., Leva, D., Rosi, M., & Casagli, N. (2014). Review of ten years of volcano deformations recorded by the ground-based InSAR monitoring system at Stromboli volcano: A tool to mitigate volcano flank dynamics and intense volcanic activity. *Earth-Science Reviews*, *139*, 317–335. https://doi.org/10.1016/j.earscirev.2014.09.011

Farina, A. (1992). *Antenna-based signal processing techniques for radar systems(Book)*. Artech House, 1992.

Feng, W., Friedt, J.-M., Nico, G., & Sato, M. (2019). 3-D ground-based imaging radar based on C-band cross-MIMO array and tensor compressive sensing. *IEEE Geoscience and Remote Sensing Letters*, *16*(10), 1585–1589. https://doi.org/10.1109/LGRS.2019.2906077

Friedlander, B. (2013). On the role of waveform diversity in MIMO radar. *Digital Signal Processing*, *23*(3), 712–721. https://doi.org/10.1016/j.dsp.2012.12.008

Han, C., Tian, W., & Mei, H. (2019). MIMO Radar Fast Imaging Algorithm Based on Sub-image Combination. *2019 6th Asia-Pacific Conference on Synthetic Aperture Radar (APSAR)*, 1–6.

Hosseiny, B., Amini, J., & Safavi-Naeini, S. (2021). Evaluating the deformation monitoring capability of a ground based SAR system with MIMO antenna. *Engineering Journal of Geospatial Information Technology*, *9*(1), 21–40. https://doi.org/10.52547/jgit.9.1.21

Hu, C., Deng, Y., & Tian, W. (2021). *Multistatic ground-based differential interferometric MIMO radar for 3D deformation measurement*. Science China Press.

Ichoku, C., Karnieli, A., Arkin, Y., Chorowicz, J., Fleury, T., & Rudant, J. P. (1998). Exploring the utility potential of SAR interferometric coherence images. *International Journal of Remote Sensing*, *19*(6), 1147–1160. https://doi.org/10.1080/014311698215658

Izumi, Y., Frey, O., Baffelli, S., Hajnsek, I., & Sato, M. (2021). Efficient Approach for Atmospheric Phase Screen Mitigation in Time Series of Terrestrial Radar Interferometry Data Applied to Measure Glacier Velocity. *IEEE Journal of Selected Topics in Applied Earth Observations and Remote Sensing*, *14*, 7734–7750. https://doi.org/10.1109/JSTARS.2021.3099873

Jin, Y., Moura, J. M. F., & O'Donoughue, N. (2010). Time reversal in multiple-input multiple-output radar. *IEEE Journal of Selected Topics in Signal Processing*, *4*(1), 210–225. https://doi.org/10.1109/JSTSP.2009.2038983

Khan, H. A., & Edwards, D. J. (2006). Doppler problems in orthogonal MIMO radars. *2006 IEEE Conference on Radar*, 4pp.

Langley, J. D. S., Hall, P. S., & Newham, P. (1993). Novel ultrawide-bandwidth Vivaldi antenna with low crosspolarisation. *Electronics Letters*, *29*(23), 2004–2005. https://doi.org/10.1049/el:19931336

Le, C. F. (2002). *Principles of radar and sonar signal processing*. Artech House.

Leva, D., Nico, G., Tarchi, D., Fortuny-Guasch, J., & Sieber, A. J. (2003). Temporal analysis of a landslide by means of a ground-based SAR interferometer. *IEEE Transactions on Geoscience and Remote Sensing*, *41*(4), 745–752. https://doi.org/10.1109/TGRS.2003.808902

Li, J., Stoica, P., & Friedlander, B. (2007). MIMO radar with colocated antennas. *Digital Signal Processing*, *23*(5), 712–721.

Luzi, G., Pieraccini, M., Mecatti, D., Noferini, L., Guidi, G., Moia, F., & Atzeni, C. (2004). Ground-based radar interferometry for landslides monitoring: Atmospheric and instrumental decorrelation sources on experimental data. *IEEE Transactions on Geoscience and Remote Sensing*, *42*(11), 2454–2466. https://doi.org/10.1109/TGRS.2004.836792

Maresca, S., Malacarne, A., Ghelfi, P., & Bogoni, A. (2021). Information diversity in coherent MIMO radars. *2021 IEEE Radar Conference (RadarConf21)*, 1–6.

Marsella, M., Proietti, C., Sonnessa, A., Coltelli, M., Tommasi, P., & Bernardo, E. (2009). The evolution of the Sciara del Fuoco subaerial slope during the 2007 Stromboli eruption: Relation between deformation processes and effusive activity. *Journal of Volcanology and Geothermal Research*, *182*(3–4), 201–213. https://doi.org/10.1016/j.jvolgeores.2009.02.002

Massonnet, D., Feigl, K., Rossi, M., & Adragna, F. (1994). Radar interferometric mapping of deformation in the year after the Landers earthquake. *Nature*, *369* (6477), 227–230. https://doi.org/10.1038/369227a0

Massonnet, D., & Rabaute, T. (1993). Radar interferometry: Limits and potential. *IEEE Transactions on Geoscience and Remote Sensing*, *31*(2), 455–464. https://doi.org/10.1109/36.214922

Meta, A., Hoogeboom, P., & Ligthart, L. P. (2007). Signal processing for FMCW SAR. *IEEE Transactions on Geoscience and Remote Sensing*, *45*(11), 3519–3532. https://doi.org/10.1109/TGRS.2007.906140

Moffet, A. (1968). Minimum-redundancy linear arrays. *IEEE Transactions on Antennas and Propagation*, *16*(2), 172–175. https://doi.org/10.1109/TAP.1968.1139138

Pieraccini, M., Miccinesi, L., Bamler, R., & Hartl, P. (1998). Ground-based radar interferometry: A bibliographic review. *Remote Sensing*, *14*(4), R1.

Prati, C., Rocca, F., Giancola, D., & Guarnieri, A. M. (1998). Passive geosynchronous SAR system reusing backscattered digital audio broadcasting signals. *IEEE Transactions on Geoscience and Remote Sensing*, *36*(6), 1973–1976. https://doi.org/10.1109/36.729370

Sammartino, P. F., Baker, C. J., & Griffiths, H. D. (2010). Range-angle dependent waveform. *2010 IEEE Radar Conference*, 511–515.

Sammartino, P. F., Baker, C. J., & Griffiths, H. D. (2013). Frequency diverse MIMO techniques for radar. *IEEE Transactions on Aerospace and Electronic Systems*, *49*(1), 201–222. https://doi.org/10.1109/TAES.2013.6404099

Sammartino, P. F., Baker, C. J., & Rangaswamy, M. (2007). Mimo Radar, Theory and Experiments. *2007 2nd IEEE International Workshop on Computational Advances in Multi-Sensor Adaptive Processing*, 101–104.

Sammartino, P. F., Baker, C. J., & Rangaswamy, M. (2008). Moving target localization with multistatic radar systems. *2008 IEEE Radar Conference*, 1–6.

Sammartino, P. F., Tarchi, D., & Baker, C. J. (2011). MIMO radar topology: A systematic approach to the placement of the antennas. *2011 International Conference on Electromagnetics in Advanced Applications*, 114–117.

Shi, X., Jiang, L., Jiang, H., Wang, X., & Xu, J. (2021). Geohazards analysis of the Litang-Batang section of Sichuan-Tibet Railway using SAR Interferometry. *IEEE Journal of Selected Topics in Applied Earth Observations and Remote Sensing*.

Soni, C., Chaudhary, A., Sharma, U., & Sharma, C. (2021). Satellite radar interferometry for DEM generation using Sentinel-1A imagery. In M.K. Sharma, V.S. Dhaka, T. Perumal, N. Dey, & J.M.R.S. Tavares (Eds.), *Innovations in Computational Intelligence and Computer Vision* (pp. 26–33). Springer. https://doi.org/10.1007/978-981-15-6067-5_4

Tarchi, D. (2003). Monitoring landslide displacements by using ground-based synthetic aperture radar interferometry: Application to the Ruinon landslide in the Italian Alps. *Journal of Geophysical Research*, *108*(B8), 1–14. https://doi.org/10.1029/2002jb002204

Tzouvaras, M. (2021). Statistical time-series analysis of interferometric coherence from sentinel-1 sensors for landslide detection and early warning. *Sensors*, *21*(20), 6799. https://doi.org/10.3390/s21206799

Van Trees, H. L. (1968). *Detection, Estimation and Modulation Theory, Part I¿* (pp. 52–74). John Wiley and Sons. Inc.

Wasowski, J., & Bovenga, F. (2022). Remote sensing of landslide motion with emphasis on satellite multi-temporal interferometry applications: An overview. *Landslide Hazards, Risks, and Disasters*, 365–438. https://doi.org/10.1016/B978-0-12-818464-6.00006-8

Wennstrom, M., Helin, M., Rydberg, A., & Oberg, T. (2001). *On the optimality and performance of transmit and receive space diversity in MIMO channels*. IEE Seminar MIMO: Communications Systems from Concept to Implementation, 2001.

Yin, D., & Zhang, F. (2020). Uniform linear array MIMO radar unitary root MUSIC Angle estimation. *2020 Chinese Automation Congress (CAC)*, 578–581. https://doi.org/10.1109/CAC51589.2020.9327698

Zebker, H. A., Rosen, P. A., Goldstein, R. M., Gabriel, A., & Werner, C. L. (1994). On the derivation of coseismic displacement fields using differential radar interferometry: The Landers earthquake. *Journal of Geophysical Research: Solid Earth*, *99*(B10), 19617–19634. https://doi.org/10.1029/94JB01179

Zhang, X., He, Z., Rayman-Bacchus, L., & Yan, J. (2015). MIMO radar transmit beampattern matching design. *IEEE Transactions on Signal Processing*, *63*(8), 2049–2056. https://doi.org/10.1109/TSP.2015.2398841